Chemical Engineering Science 266 (2023) 118290

Contents lists available at ScienceDirect

Chemical Engineering Science

journal homepage: www.elsevier.com/locate/ces

Understanding mechanisms of pyridine oxidation with ozone addition via reactive force field molecular dynamics simulations

Zhongze Bai [a], Xi Zhuo Jiang [b,*], Kai H. Luo [a,*]

[a] Department of Mechanical Engineering, University College London, Torrington Place, London WC1E 7JE, UK
[b] School of Mechanical Engineering and Automation, Northeastern University, Shenyang, Liaoning 110819, PR China

HIGHLIGHTS

- The first ReaxFF MD study on the influence of ozone on pyridine combustion.
- Revealing reaction pathways for pyridine combustion with and without ozone.
- Explaining how ozone affects pyridine combustion products at the atomic level.

ARTICLE INFO

Article history:
Received 27 June 2022
Received in revised form 13 September 2022
Accepted 6 November 2022
Available online 11 November 2022

Keywords:
Pyridine oxidation
Ozone assisted combustion
Reactive force field
Molecular dynamics
NOx

ABSTRACT

Ozone assisted combustion is a promising method to control combustion, ignition and pollutant formation. In this study, we investigated the ozone behaviours in fuel-NOx control through reactive force field (ReaxFF) molecular dynamics (MD) simulations of pyridine (a main nitrogen-containing compound in coal) oxidation under different ozone concentrations. The results show that ozone enhances the pyridine combustion process and facilitates the conversion of CO to CO_2 and NO to NO_2. Ozone participates in the reactions with intermediates and promotes the generation of active particles like OH, HO_2, HO_3 and H_2O_2. This research reveals mechanisms, at the atomic level, for the effects of main products formation during pyridine oxidation under different levels of ozone addition. The present study provides the scientific base for the control of NOx emissions through ozone assisted combustion technology.

1. Introduction

The nitrogen oxides (NOx) emissions from the coal combustion cause serious environmental problems (Bowman, 1992), and thus modern control technologies for combustion are desired to reduce nitrogenous pollutants. The NOx emissions from combustion processes are mostly nitric oxide (NO) with smaller amounts of nitrogen dioxide (NO_2) (Glarborg et al., 2003). NO_2 can be easily removed by water due to its high solubility (Mok and Lee, 2006). By contrast, due to its low solubility, NO in exhaust gases has to be removed by selective catalytic reduction (SCR) with high operation costs (Mok and Lee, 2006). Ozone (O_3), one of the strongest oxidizers, has the ability to improve combustion performance (such as ignition, flame propagation and flame stabilization) and influence the conversion from NO to NO_2 by modifying fuel oxidation pathways (Sun et al., 2019). Thus, O_3 addition can be a feasible and promising method to control NOx emissions from coal combustion.

There are numerous studies focusing on the influence of O_3 on ignition (Yamada et al., 2005; Foucher et al., 2013), flame propagation (Gao et al., 2015; Gluckstein et al., 1955) and flame stabilization (Zhang et al., 2016; Weng et al., 2015) in fuel combustion. Tachibana and co-workers carried out experiments to explore the effects of O_3 on combustion of compression ignition engines (Tachibana et al., 1991). Results indicate that O_3 can decrease CO, C_nH_m, and soot, but increase NOx emissions. The same conclusion is also drawn by Nasser and co-workers when they investigated the O_3 influence on the combustion characteristics of internal combustion engines (Nasser et al., 1998). Previous studies have demonstrated O_3 addition can change the exhaust emissions from fuel combustion effectively. However, the effects of O_3 addition on emissions of pollutants from fuel combustion are less explored. There are also some unsolved fundamental questions. For instance, the underlying mechanisms of O_3 influence on NOx formation from combustion are still unclear. Moreover, the composition of NOx

* Corresponding authors.
E-mail addresses: jiangxz@mail.neu.edu.cn (X.Z. Jiang), k.luo@ucl.ac.uk (K.H. Luo).

https://doi.org/10.1016/j.ces.2022.118290
0009-2509/

emissions under varying O_3 concentrations was not investigated in above research, which would affect the operating costs in the NOx reduction process.

The underlying mechanisms are difficult to be determined by current experimental techniques due to the difficulty in obtaining all the intermediates (Liu and Guo, 2017). Atomistic computational simulations can reveal the reaction mechanism at the molecular level and obtain reaction information that cannot be obtained by experimental measurement. The main atomistic simulation methods include quantum mechanics (QM) and molecular dynamics (MD). QM methods can simulate chemical reactions accurately. However, the simulated system is usually smaller than 100 atoms as QM is computationally expensive to simulate large systems (Feng et al., 2019; Jiang and Luo, 2021; Jiang et al., 2019). Classical MD methods can simulate large-scale systems of constitutive atoms/molecules (Jiang et al., 2020), but they are not amenable to chemical reactions. The reactive force field molecular dynamics (ReaxFF MD) simulation combines the capability of QM and affordable computational cost of classical MD methods, which can be used to simulate the chemical reaction process of complex systems. In the combustion of coal, nitrogen oxides mainly come from the oxidation of nitrogen-containing compounds with pyridinic and pyrrolic structures (Glarborg et al., 2003). The major forms of nitrogen groups in coal are pyrrolic-N (N-5) of 50–80 % and pyridinic-N (N-6) of 20–40 % (Zhang et al., 2021). According to a previous study (Axworthy et al., 1978), pyridine and pyrrole share similar NOx formation mechanisms, and pyridine (C_5H_5N) - the main nitrogen-containing compound in coal (Solomon and Colket, 1978; Nelson et al., 1991; Bai et al., 2021) - is chosen as the target molecule during our ReaxFF MD simulations in this study.

The aim of this study is to investigate the effects of O_3 on the emissions of pollutants from C_5H_5N oxidation via a series of ReaxFF MD simulations. Firstly, time evolutions of main reactants are studied. Then, the effects of O_3 on the yields of the reactions are explored. Finally, the elementary reactions generating principal products are revealed during C_5H_5N oxidation under varying O_3 concentrations.

2. Methods

The ReaxFF MD is originally developed by van Duin and coworkers (Van Duin et al., 2001), which employs a bond-order formalism in conjunction with polarizable charge descriptions to determine both reactive and non-reactive interactions between atoms (Senftle et al., 2016). The energy function in the ReaxFF force field is shown in Eq. (1):

$$E_{system} = E_{bond} + E_{over} + E_{angle} + E_{tors} + E_{vdWaals} + E_{Coulomb} + E_{Specific} \quad (1)$$

More details of the ReaxFF formalism and development are shown in (Senftle et al., 2016).

All the ReaxFF MD simulations are carried out using the REAXC package in the Large-scale Atomic/Molecular Massively Parallel Simulator (LAMMPS) platform (Thompson et al., 2022), with the C/H/O/N force field (Zhang et al., 2009; Zhang et al., 2009). To investigate the O_3 addition on C_5H_5N combustion, seven periodic systems with different numbers of O_3 ranging from 0 to 240 are built with a density of 0.3 g/cm^3. To facilitate analysis, the ratio of the number of O_3 molecules, $n(O_3)$, to the number of C_5H_5N molecules, $n(C_5H_5N)$, is defined as α. The numbers of C_5H_5N and O_2 are 80 and 540 in all systems, respectively. The details of all cases are shown in Table 1. The data of case 1 are shared with our previous work (Bai et al., 2023). A typical initial configuration for the simulated system is illustrated in Fig. 1.

Table 1
Details of simulation systems.

NO.	Number of molecules	α	Box length (Å)
1	$80C_5H_5N/540O_2/0O_3$	0	50.7446
2	$80C_5H_5N/540O_2/40O_3$	0.5	52.0846
3	$80C_5H_5N/540O_2/80O_3$	1	53.3589
4	$80C_5H_5N/540O_2/120O_3$	1.5	54.5751
5	$80C_5H_5N/540O_2/160O_3$	2	55.7394
6	$80C_5H_5N/540O_2/200O_3$	2.5	56.8569
7	$80C_5H_5N/540O_2/240O_3$	3	57.9322

The canonical (NVT) ensemble is used for all the MD simulations. The time step and bond order cutoff are 0.1 fs and 0.3, respectively. Before the reactive simulations, each system undergoes energy minimization and equilibration at 500 K for 100 ps to optimize the initial geometric configuration. Then, the system temperature increases to 2600 K (with a heating rate of 10 K/ps) and the temperature is kept constant at 2600 K. The physical time of reaction is 1000 ps for every individual simulation.

In data analysis, the reaction pathways are obtained by Chemical Trajectory Analyzer (ChemTraYzer) scripts (Döntgen et al., 2015). The visualizations are produced by Visual Molecular Dynamics (VMD) (Humphrey et al., 1996). The net flux (NF) is the number difference between the forward reaction and the number of the reverse reaction (Arvelos and Hori, 2020). The data in this study are the average results of the three replica simulations. Error bars in all figures are Standard Error (SE) of three replicas.

3. Results

3.1. Time evolution of reactants

Fig. 2 shows the time evolution of main reactants with α ranging from 0.5 to 3. The comparison of Fig. 2a and 2b illustrates that the reaction rate of C_5H_5N increases as the number of O_3 additives rises, which demonstrates that O_3 can enhance the combustion process. According to Fig. 2c, the number of O_2 decreases all the way in the O_3-free case; by contrast, in the O_3 cases, the number of O_2 first reaches a peak and then declines. The peak amount of O_2 also rises with α values. Fig. 2d shows that O_3 molecules are completely consumed at the first 100 ps. Fig. 2c and 2d suggest that O_3 related reactions may account for the increase of O_2 amount at the initial stage. To further confirm such a conclusion, more details of reaction mechanisms of O_3 are needed, as shown in the subsequent section.

3.2. Reaction mechanisms of O_2 and O_3

To further explain O_3 influence on the consumption rates of main reactants, reaction mechanisms of O_2 and O_3 are investigated in this section. O_2 molecules react with intermediates forming oxygen-containing species and HO_2 via R1 and R2, respectively.

$$C_xH_yO_zN_n + O_2 \rightarrow C_xH_yO_{z+2}N_n \quad (R1)$$

$$C_xH_yO_zN_n + O_2 \rightarrow C_xH_{y-1}O_zN_n + HO_2 \quad (R2)$$

The oxygen-containing species can also decompose by subtracting O and OH radicals:

$$C_xH_yO_zN_n \rightarrow C_xH_yO_{z-1}N_n + O \quad (R3)$$

$$C_xH_yO_zN_n \rightarrow C_xH_{y-1}O_{z-1}N_n + OH \quad (R4)$$

O_2 molecules react with H and OH radicals forming HO_2 and HO_3 via reactions:

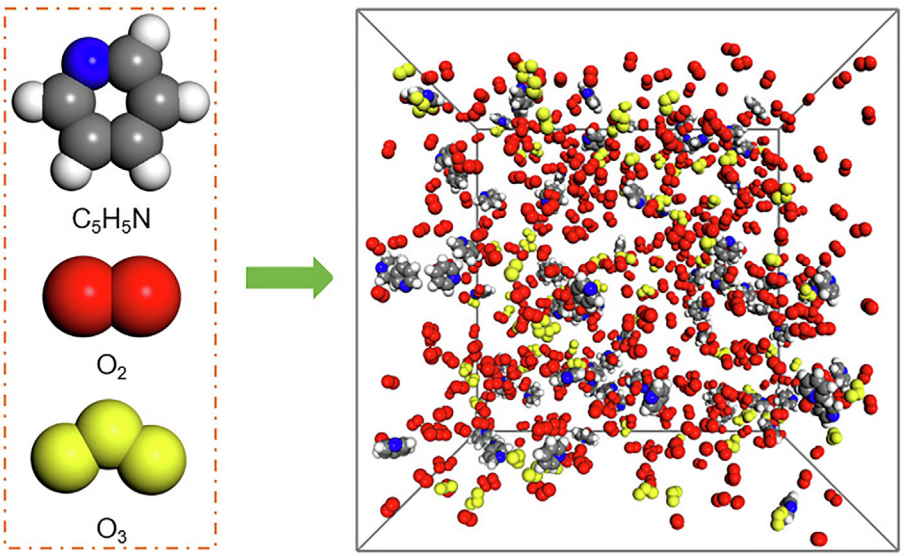

Fig. 1. Initial configuration of $C_5H_5N/O_2/O_3$ system. Yellow: O_3 molecules. Red: O_2 molecules. Dark grey: C atom. Light grey: H atom. Blue: N atom.

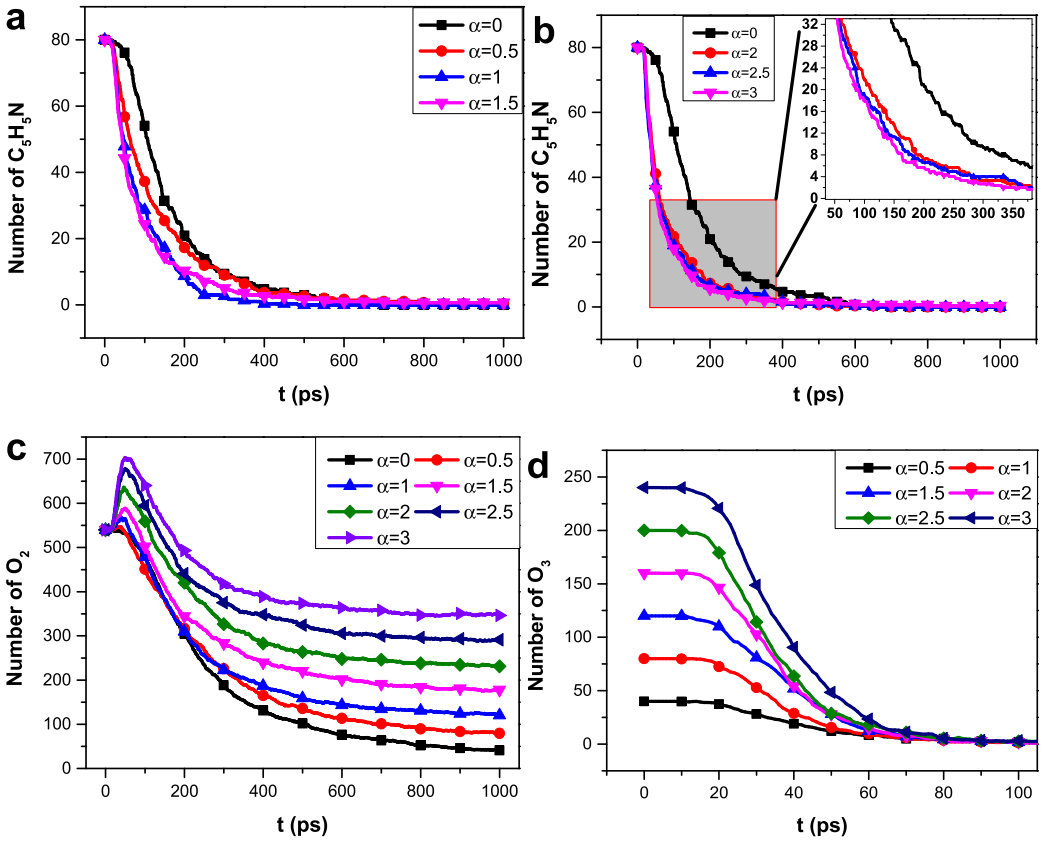

Fig. 2. Time evolution of main reactants. (a) C_5H_5N (α = 0–1.5); (b) C_5H_5N (α = 0&2–3); (c) O_2; (d) O_3.

$$O_2 + H \rightarrow HO_2 \quad (R5)$$

$$O_2 + OH \rightarrow HO_3 \quad (R6)$$

H_2O_2 is produced through reactions of HO_2 between H_2O and HO_2, as shown in R7 and R8:

$$HO_2 + H_2O \rightarrow H_2O_2 + OH \quad (R7)$$

$$HO_2 + HO_2 \rightarrow H_2O_2 + O_2 \quad (R8)$$

As for OH radicals, besides R4 and R7, the reaction of H_2O and O and the decomposition of H_2O_2 both contribute to the generation of OH radicals.

$$H_2O + O \rightarrow HO + HO \quad (R9)$$

$$H_2O_2 \rightarrow HO + HO \quad (R10)$$

The active radicals (OH, HO_2, HO_3 and H_2O_2) originated from O_2 will finally participate in the reactions that form key products, like CO, CO_2, NO, NO_2 and N_2. In the C_5H_5N combustion with O_3 addition, the O_3 related reactions include three parts: thermal decomposition, reactions with hydrocarbons and reactions with other key radicals (Sun et al., 2019). The thermal decomposition of O_3 releases O_2 and O via R11:

$$O_3 \rightarrow O_2 + O\,() \quad (R11)$$

In the reactions of O_3 and hydrocarbons, O_2 and further oxidated intermediates are formed through R12:

$$C_xH_yO_zN_n + O_3 \rightarrow C_xH_yO_{z+1}N_n + O_2 \quad (R12)$$

The reactions of O_3 and radicals are related to O_3 concentrations. O_3 will react with OH to form HO_2 as follows:

$$HO_2 + O_3 \rightarrow O_2 + O_2 + OH\,() \quad (R13)$$

$$OH + O_3 \rightarrow O_2 + HO_2\,() \quad (R14)$$

$$HO_2 + O_3 \rightarrow O_2 + HO_3 \quad (R15)$$

O_3 molecules react with O and generate O_2 through R16 in cases with $\alpha = 1.5 \sim 3$. When α is higher than 2, O_3 will react with H and O_3 by R17 and R18.

$$O_3 + O \rightarrow O_2 + O_2\,() \quad (R16)$$

$$O_3 + H \rightarrow O_2 + HO\,() \quad (R17)$$

$$O_3 + O_3 \rightarrow O_2 + O_2 + O_2 \quad (R18)$$

As discussed above, O_3 molecules can promote the oxidation process of reactants directly. In addition, O_3 can also facilitate the formation O_2, OH, HO_2, HO_3 and H_2O_2, which accounts for the increasing trends of O_2 molecules in the O_3 cases (Fig. 2c) and maximum numbers of OH, HO_2, HO_3 and H_2O_2 with α (Fig. 3). Moreover, the increase in active radicals enhances the combustion process resulting in the faster consumption rates of C_5H_5N molecules, as shown in Fig. 2a and 2b.

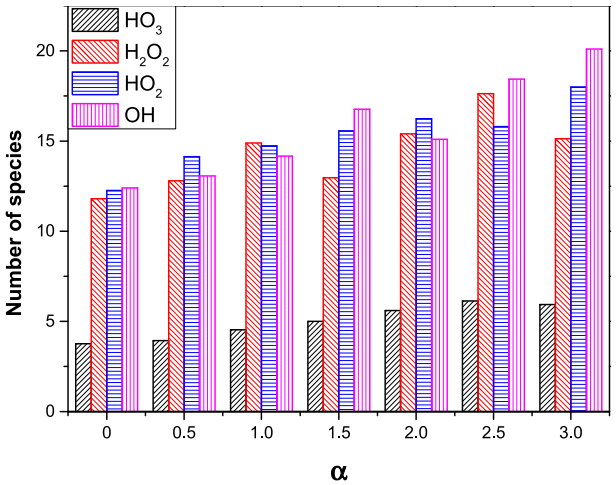

Fig. 3. Maximum numbers of HO_3, H_2O_2, HO_2 and HO.

3.3. Effects of O_3 on the production of main products

For nitrogen-free products, Fig. 4a and 4b suggest that the number of CO decreases with increasing α, however, the increase of O_3 enhances CO_2 production during C_5H_5N combustion when α changes from 0 to 1.5. When α is greater than 1.5, the changes of CO and CO_2 production with α are not significant. In Fig. 4c and 4d, the yields of NO and NO_2 show a similar trend with CO and CO_2, respectively. As shown in Fig. 4f, the number of N_2 decreases as the number of O_3 rises when α is greater than 0.5. By contrast, NOx presents an opposite trend with N_2 as shown in Fig. 4e. The influence of O_3 on the generation of NOx and CO agrees well with previous studies (Tachibana et al., 1991; Nasser et al., 1998).

In this section, the effects of O_3 addition on the yield of products are analysed. To further identify the effects of O_3 on the underlying mechanisms of key products generation, the reaction pathways of nitrogen-containing and nitrogen-free products are scrutinized in Section 3.4 and 3.5, respectively.

3.4. Reaction pathways of CO and CO_2

There are two stages for the generation of nitrogen-containing products during the C_5H_5N oxidation. The initial formation of CO and CO_2 is from the thermal decomposition of oxygen-containing intermediates as shown in R19 and R20. Then, CO will be converted to CO_2 through the reactions with reactive radicals (O_2, O_3, HO_2, HO_3 and H_2O_2).

$$C_xH_yO_zN_n \rightarrow C_{x-1}H_yO_{z-1}N_n + CO \quad (R19)$$

$$C_xH_yO_zN_n \rightarrow C_{x-1}H_yO_{z-2}N_n + CO_2 \quad (R20)$$

As shown in Fig. 5, the effects of O_3 on the ratios of R19 and R20 occurrence are insignificant, with individual percentages of 63 % and 37 %, respectively. The result indicates that the increase of CO_2 production with O_3 addition is by the promotion of conversion from CO to CO_2 during C_5H_5N combustion. Table 2 illustrates NF of main elementary pathways linked with conversion from CO to CO_2. Results indicate that O_3 promotes the conversion from CO to CO_2 significantly when α is less than 1.5, but the profiles of CO and CO_2 almost remain the same with $\alpha = 1.5 \sim 3$, which is in good agreement with O_3 influence on the yields of CO and CO_2 in Fig. 4.

There are six pathways for CO consumption, that is, CO → CO_2, CO → CO_3, CO → CHO_2, CO → CHO_3, CO → CHO_4 and CO → CO_4. As shown in Table 2, the NF of CO → CO_3 shows an upward trend as α increases. By contrast, O_3 has insignificant influence on the conversion from CO to CHO_3. The reactions generating CO_3 and CHO_3 from CO are through R21 and R22 as shown in Table 3.

The pathways of CO to CO_2 and CHO_2 show similar trends, which peak at $\alpha = 1.5$ and 0.5, respectively, and then decrease with the increase of O_3 addition in the C_5H_5N oxidation. The channels converting from CO to CHO_2 are shown in R23 to R25.

The reaction of CO and OH dominates in the formation of CHO_2. CO can be converted to CO_2 via six ways as demonstrated in R26 to R31.

When α is 0 or 3, the reaction CO with H_2O_2 forming CO_2 is observed (R32). CO molecules will react with O_3 producing CO_2 in all O_3 addition cases (R33).

Moreover, O_3 promotes the reactions of R29, R31 and R33 and enhances the conversion from CO to CO_2 with $\alpha = 0$–1.5. When α is larger than 1.5, the NF of reactions R26, R27 and R31 is reduced, resulting in the reduction of the conversion from CO to CO_2. Additionally, CO will be converted to CHO_4 and CO_4 at $\alpha = 3$ via R34 and R35.

Mutual transformation pathways are found for key intermediates generated by R21 to R35 (such as $CHO_2 \rightarrow CHO_4$, $CO_3 \rightarrow CHO_3$).

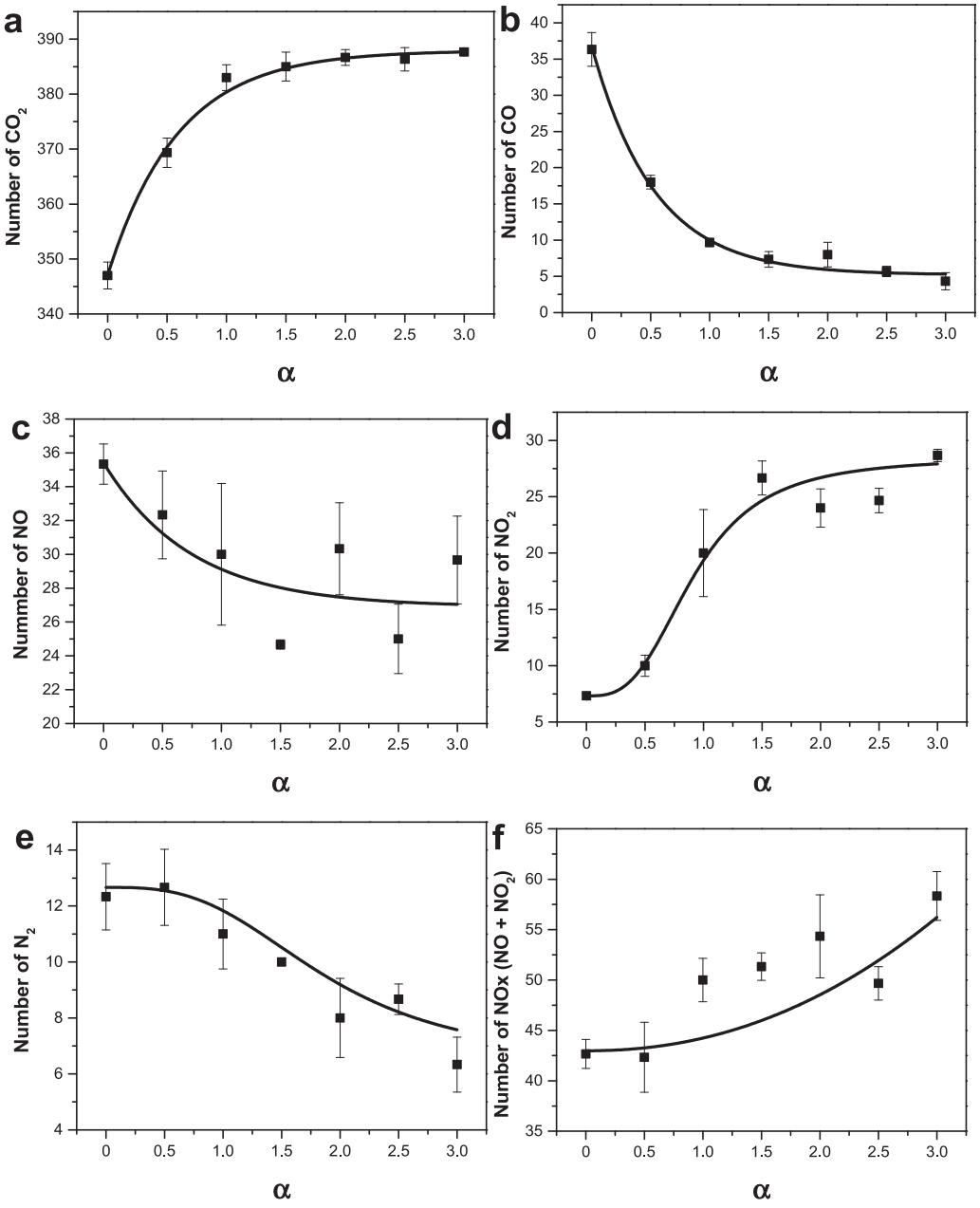

Fig. 4. Effects of O_3 on the yield of main products. (a) CO_2; (b) CO; (c) NO; (d) NO_2; (e) N_2; (f) NOx.

Here we mainly focus on the transfer pathways of CO_2 generation. Table 3 shows the NF of pathways generating CO_2, which are CO → CO_2, CO_3 → CO_2, CHO_2 → CO_2, CHO_3 → CO_2, CHO_4 → CO_2 and CO_4 → CO_2. Overall, O_3 promotes the conversion from CO, CHO_3, CHO_4 to CO_2. The NF of pathway CHO_2 → CO_2 peaks at α = 0.5, and slightly decreases as α rises to 3. The NFs of the pathway from CO_4 to CO_2 are zero with α = 0 ∼ 1.5, however O_3 enhances the CO_2 formation when α is higher than 1.5.

Regarding the pathway CO_3 to CO_2, CO_2 is generated by thermal decomposition of CO_3 and reactions of CO_3 with H_2O, OH, O_2, CO and HO_2, as shown in R36 to R41. R36 to R39 are commonly observed in all cases. R40 occurs in α = 0 ∼ 1.5, 2 and 2.5 cases and R41 occurs with α from 1 to 3. In addition, the increase in NF of CO_2 formation by CO_3 with increasing α is due to the enhancement of R36 by O_3 molecules. CHO_2 conversion to CO_2 is via channels R42 to R46.

R42 - R44 take place in all conditions. R45 occurs when α is 0 and 1 ∼ 2. R46 happens in α = 0.5, 1, 2.5 and 3 cases. R42 is the main pathway from CHO_2 to CO_2. The conversion from CHO_3 to CO_2 is via R47 and R48, and R48 only occurs in the α = 1, 2 and 3 cases. The rising O_3 addition promotes R48, which is the main reason for the upward profile of CHO_3 → CO_2. The pathways of CO_2 formation by CHO_4 and CO_4 are shown in R49 and R50, respectively.

3.5. Reaction pathways of NO, NO_2 and N_2

Fig. 6 illustrates the transfer pathways of NO and NO_2 under different α values. The starting radicals of CNO, HNO, CNO_2 and $CHNO_3$ are important precursors of NOx formation during C_5H_5N oxidation. More details of C_5H_5N oxidation mechanisms can be found in previous studies (Luo et al., 2019; Ikeda et al., 2000). Dur-

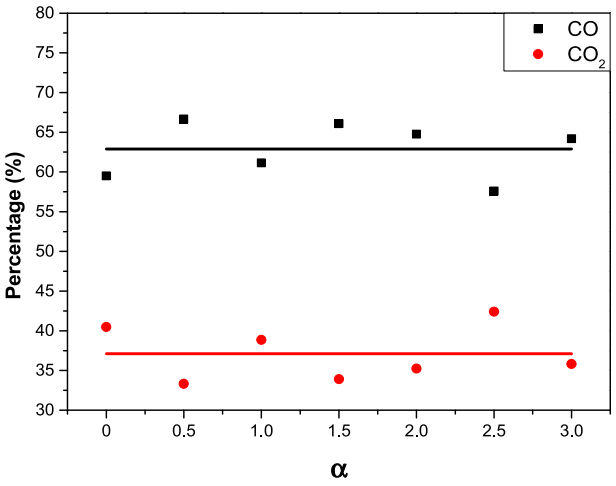

Fig. 5. Percentages of CO and CO_2 generated from oxygen-containing intermediates decomposition.

ing NO generation, the pathways from CNO_3, CNO_2, HNO and $CHNO_3$ to NO occur in all conditions, and $NO_3 \rightarrow NO$ is observed in the $\alpha = 0.5 \sim 2$ and 3 cases. Four pathways lead to NO consumption: $NO \rightarrow HNO_3$, $NO \rightarrow NO_2$, $NO \rightarrow HNO_2$ and $NO \rightarrow CN_2O_2$. The channel $NO \rightarrow CN_2O_2$ only takes place with $\alpha = 0 \sim 2.5$. Besides, HNO_3 and HNO_2 are also essential intermediates for NO_2 formation. When α ranges from 0.5 to 3, channels $HNO_4 \rightarrow NO_2$ and $CNO_2 \rightarrow CNO_4 \rightarrow NO_2$ are detected, and HNO_4 mainly comes from the conversion of HNO_3, HNO_2 and NO_3. Regarding NO_2 consumption, the pathways of NO_2 to NO_3 and CNO_3 occur in cases with $\alpha = 0.5 \sim 1.5$ & $2.5 \sim 3$ and $0 \sim 1$ & 2 & 3, respectively.

To further explain O_3 influence on the yields of NO and NO_2, we explored the NF analysis of those products as shown in Table 4. The total net NF of NO presents a downward trend, which agrees well with the yield of NO under different O_3 concentrations. Besides, the NO generation is promoted slightly by the increasing α value; by contrast, O_3 enhances NO consumption significantly. Thus, it can be concluded that O_3 influence on NO consumption plays a dominant role in NO production. Besides, the conversions from NO to NO_2 and HNO_2 increase with α values. The NF of channel $NO \rightarrow HNO_3$ first decreases until it reaches the lowest point at $\alpha = 1.5$, and then increases. Regarding the conversion from NO to CN_2O_2, the change in NFs is not significant when α increases from 0 to 1, but decreases when α is higher than 1.

As shown in Table 5, the conversion between NO and NO_2 is through R51 to R58. Among them, R51, R52, R54 and R55 are observed in cases with O_3 addition. R53 occurs in $\alpha = 0 \sim 2.5$ cases. R56 takes place with α of 1 and 3. R57 is observed in $\alpha = 0.5 \sim 3$ cases. R58 only happens in the $\alpha = 2$ case. When α ranges from $0 \sim 1.5$, R51, R52 and R54 play key roles in the yield of NO. Specifically, O_3 promotes the conversion from NO to NO_2 via R52 and R54, but weakens the channel $NO_2 \rightarrow NO$ through R51, accounting for the increase of NO consumption via the channel $NO \rightarrow NO_2$ when α is less than 1.5. As α is larger than 1.5, O_3 has insignificant influence on R51, R52 and R54, but it promotes the overall generation of NO_2.

The reactions of $NO \rightarrow CN_2O_2$ and $NO \rightarrow HNO_3$ are presented in R59 and R60, respectively. The pathway from NO to HNO_2 is via R61 to R64. Among them, R61 and R62 are spotted in all cases. R63 is observed in $\alpha = 0.5$ and $2 \sim 3$ cases. R64 is found in $\alpha = 0.5 \sim 1$ and $2 \sim 3$ conditions. In addition, $NO + HO \rightarrow HNO_2$ (R62) plays dominant roles in the conversion from NO to HNO_2.

Regarding the NFs of NO_2 consumption and formation, the total net NF of NO_2 is in good consistence with NO_2 production at various O_3 conditions. Besides, the NF of NO_2 almost remains the same, thus the NO_2 amount is determined by the NF of NO_2 generation. Also, O_3 promotes the conversions of NO_2 generation from NO and HNO_4. The NF of the pathway $HNO_3 \rightarrow NO_2$ shows a downward trend with $\alpha = 0 \sim 1$, but this channel is enhanced by O_3 when α is larger than 1. As to the pathways $HNO_2 \rightarrow NO_2$ and $CNO_2 \rightarrow NO_2$, the NF of these reactions increases to the peak at $\alpha = 1.5$ and then decreases. The results indicate that the promotion effects of O_3 on NO_2 generation from NO, HNO_2, CNO_4 and HNO_4 cause the increase of NO_2 amount with α ranging from 0 to 1.5. Moreover, the inhibition of NO_2 formation from HNO_2 and CNO_4 causes the number of NO_2 to almost remain the same when α is from 1.5 to 3.

The reactions of NO_2 formation from HNO_3, CNO_4 and HNO_4 are shown in R65 to R67. As to conversion of HNO_2 to NO_2 by channels R68 to R70, the reaction between HNO_2 and O_2 (R69) is the main cause for NO_2 formation.

As for the N_2 generation, $C_2N_2O_2$ is the key precursor generated by R71. Two pathways for N_2, are $C_2N_2O_2 \rightarrow N_2$ (R72) and $C_2N_2O_2 \rightarrow CN_2O \rightarrow N_2$ (R73 to R74). The increase of O_3 addition during C_5H_5N combustion inhibits the conversion from $C_2N_2O_2$ and CN_2O to N_2 resulting in the decrease of N_2 formation with α value rising.

3.6. Discussion

When O_3 is added in the C_5H_5N combustion, it affects the consumption rates of reactants and yields of productions by reacting with intermediates directly and promotes the formation of active radicals like OH, HO_2, HO_3 and H_2O_2.

According to the current study, O_3 shows satisfactory performance on reducing CO and NO emissions with $\alpha = 0 \sim 1.5$. The decrease of NO emissions can reduce operating costs in exhaust

Table 2
Net flux (NF) of main elementary pathways linked with conversion from CO to CO_2.

Pathways	0	0.5	1	1.5	2	2.5	3
$CO \rightarrow CO_2$	171	164	165	181	178	151	155
$CO \rightarrow CO_3$	259	273	280	283	312	323	310
$CO \rightarrow CHO_2$	126	147	143	133	121	121	125
$CO \rightarrow CHO_3$	21	24	23	26	24	23	26
$CO \rightarrow CHO_4$	0	0	0	0	0	0	7
$CO \rightarrow CO_4$	0	0	0	0	0	0	4
Total CO consumption	577	608	611	623	635	618	627
$CO \rightarrow CO_2$	171	164	165	181	178	151	155
$CO_3 \rightarrow CO_2$	163	223	215	232	232	259	232
$CHO_2 \rightarrow CO_2$	101	155	106	138	123	118	124
$CHO_3 \rightarrow CO_2$	65	70	64	76	76	71	75
$CHO_4 \rightarrow CO_2$	10	12	28	11	19	38	27
$CO_4 \rightarrow CO_2$	0	5	2	1	9	15	30
Total CO_2 generation	510	629	580	639	637	652	643

Table 3
Summary of reactions on the conversion from CO to CO_2.

ID	Reactions	ID	Reactions
R21	$CO + O_2 \rightarrow CO_3$	R36	$CO_3 \rightarrow CO_2 + O$
R22	$CO + HO_2 \rightarrow CHO_3$	R37	$CO_3 + H_2O \rightarrow CO_2 + HO + HO$
R23	$CO + OH \rightarrow CHO_2$	R38	$CO_3 + OH \rightarrow CO_2 + HO_2$
R24	$CO + H_2O_2 \rightarrow CHO_2 + HO$	R39	$CO_3 + O_2 \rightarrow CO_2 + O_3$
R25	$CO + HO_3 \rightarrow O_2 + CHO_2$	R40	$CO_3 + CO \rightarrow CO_2 + CO_2$
R26	$CO + HO_2 \rightarrow CO_2 + HO$	R41	$CO_3 + HO_2 \rightarrow CO_2 + O_2 + HO$
R27	$CO + O_2 \rightarrow CO_2 + O$	R42	$CHO_2 + O_2 \rightarrow CO_2 + HO_2$
R28	$CO + NO_2 \rightarrow CO_2 + NO$	R43	$CHO_2 \rightarrow CO_2 + H$
R29	$CO + O_2 + HO \rightarrow CO_2 + HO_2$	R44	$CHO_2 + HO \rightarrow H_2O + CO_2$
R30	$CO + O \rightarrow CO_2$	R45	$CHO_2 + H_2O_2 \rightarrow H_2O + CO_2 + HO$
R31	$CO + OH \rightarrow CO_2 + H$	R46	$O_2 + CHO_2 \rightarrow CO_2 + HO + O$
R32	$CO + H_2O_2 \rightarrow H_2O + CO_2$	R47	$CHO_3 \rightarrow CO_2 + HO$
R33	$CO + O_3 \rightarrow CO_2 + O_2$	R48	$CHO_3 + O_2 \rightarrow CO_2 + HO_3$
R34	$CO + O_2 + HO \rightarrow CHO_4$	R49	$CHO_4 \rightarrow CO_2 + HO_2$
R35	$CO + O_3 \rightarrow CO_4$	R50	$CO_4 \rightarrow CO_2 + O_2$

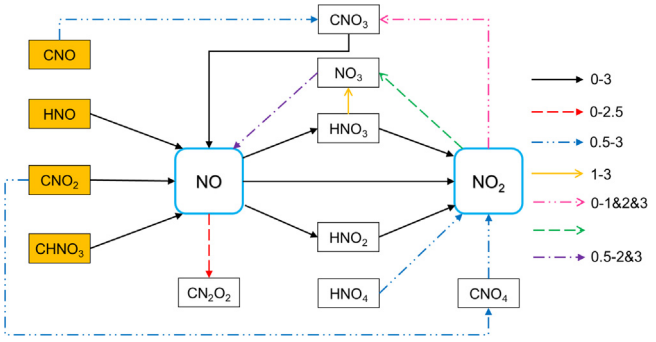

Fig. 6. Effects of O_3 on the transfer pathways of NO and NO_2. The particles in the yellow box are the starting intermediates. The numerical values in the figure are values of α.

gas treatment by the selective catalytic reduction (SCR) technology, where ammonia is used to reduce NO to N_2 with expensive catalysts. Meanwhile, O_3 promotes the conversion from NO to NO_2 resulting in increased NO_2 emissions, which can be removed by water. However, O_3 addition increases NOx (the total of NO and NO_2 emissions) emissions by inhibiting the N_2 formation, which is in consistence with previous studies (Tachibana et al., 1991; Nasser et al., 1998). Thus, the O_3 addition in combustion systems should be well designed in practice.

Table 5
Summary of reactions related to NO, NO_2 and N_2.

ID	Reactions	ID	Reactions
R51	$CO + NO_2 \rightarrow CO_2 + NO$	R63	$HNO_2 + HO_2 \rightarrow H_2O + O_2 + NO$
R52	$HO_2 + NO \rightarrow HO + NO_2$	R64	$O_2 + HNO_2 \rightarrow HO_3 + NO$
R53	$H_2O_2 + NO \rightarrow H2O + NO_2$	R65	$HNO_3 \rightarrow HO + NO_2$
R54	$NO + O \rightarrow NO_2$	R66	$CNO_4 \rightarrow CO_2 + NO_2$
R55	$H + NO_2 \rightarrow NO + HO$	R67	$HNO_4 \rightarrow HO_2 + NO_2$
R56	$CO_3 + NO \rightarrow CO_2 + NO_2$	R68	$HNO_2 + HO \rightarrow H_2O + NO_2$
R57	$HO_2 + NO_2 \rightarrow O_2 + NO + HO$	R69	$HNO_2 + O_2 \rightarrow HO2 + NO_2$
R58	$NO + O_3 \rightarrow O_2 + NO_2$	R70	$HNO_2 \rightarrow H + NO_2$
R59	$NO + CNO \rightarrow CN_2O_2$	R71	$CNO + CNO \rightarrow C_2N_2O_2$
R60	$NO + HO_2 \rightarrow HNO_3$	R72	$C_2N_2O_2 \rightarrow N_2 + 2CO$
R61	$H_2O_2 + NO \rightarrow HNO_2 + HO$	R73	$C_2N_2O_2 \rightarrow CN_2O + CO$
R62	$NO + HO \rightarrow HNO_2$	R74	$CN_2O \rightarrow N_2 + CO$

4. Conclusions

ReaxFF MD simulations are performed to investigate the effects of ozone on pyridine oxidation. Time evolutions of main species suggest that ozone enhances the pyridine combustion. In addition, the chemical reactions of ozone are identified and quantified. The influence of ozone on the yields of products is explored, and results suggest that ozone facilitates the conversion from CO to CO_2 and NO to NO_2. Finally, we reveal the underlying mechanisms at the atomic level for products generation during pyridine oxidation with varying amount of ozone addition. This research demonstrates that ReaxFF MD is a promising method to reveal reaction mechanisms of fuel-NOx formation and provides theoretical guidance on the NOx control by O_3 assisted combustion of fossil fuels. The study contributes to a deeper understanding of the role of ozone in pyridine oxidation, which may be helpful to reducing NOx and CO emissions effectively.

Table 4
Net flux (NF) of main elementary pathways linked with NO, NO_2 and N_2.

Pathways	0	0.5	1	1.5	2	2.5	3
$CNO_2 \rightarrow NO$	90	101	113	112	117	96	127
$HNO \rightarrow NO$	13	18	12	6	11	11	25
$CHNO_3 \rightarrow NO$	14	6	11	9	2	9	5
$CNO_3 \rightarrow NO$	12	6	12	9	6	5	6
$NO_3 \rightarrow NO$	0	5	1	1	9	0	−2
NO generation	129	136	149	137	145	121	161
$NO \rightarrow CN_2O_2$	8	7	9	2	1	4	0
$NO \rightarrow NO_2$	3	10	38	18	27	22	33
$NO \rightarrow HNO_3$	17	16	7	8	5	17	24
$NO \rightarrow HNO_2$	2	−2	32	51	24	53	32
NO consumption	30	31	86	79	57	96	89
Net NO generation	99	105	63	58	88	25	72
$HNO_3 \rightarrow NO_2$	13	10	1	14	6	11	24
$HNO_2 \rightarrow NO_2$	1	12	17	44	18	26	25
$CNO_4 \rightarrow NO_2$	0	9	13	6	10	12	8
$HNO_4 \rightarrow NO_2$	0	1	2	−5	8	2	8
NO_2 generation	17	42	71	77	69	73	98
$NO_2 \rightarrow CNO_3$	7	8	10	0	5	0	10
$NO_2 \rightarrow NO_3$	0	4	−2	−1	0	7	−1
NO_2 consumption	7	12	8	−1	5	7	9
Net NO_2 generation	10	30	63	78	64	66	89
$CN_2O \rightarrow N_2$	5	11	7	4	0	5	0
$C_2N_2O_2 \rightarrow N_2$	7	5	7	6	7	0	0
$N_2O \rightarrow N_2$	0	0	0	0	0	0	2
N_2 formation	12	16	14	10	7	5	2

CRediT authorship contribution statement

Zhongze Bai: Conceptualization, Methodology, Software, Investigation, Data curation, Visualization, Writing – original draft. **Xi Zhuo Jiang:** Supervision, Writing – review & editing. **Kai H. Luo:** Supervision, Funding acquisition, Resources, Project administration, Writing – review & editing.

Data availability

Data will be made available on request.

Declaration of Competing Interest

The authors declare that they have no known competing financial interests or personal relationships that could have appeared to influence the work reported in this paper.

Acknowledgements

Support from the UK Engineering and Physical Sciences Research Council under the project "UK Consortium on Mesoscale Engineering Sciences (UKCOMES)" (Grant No. EP/R029598/1) is gratefully acknowledged. This work made use of computational support by CoSeC, the Computational Science Centre for Research Communities, through UKCOMES.

References

Arvelos, S., Hori, C.E., 2020. ReaxFF study of ethanol oxidation in O_2/N_2 and O_2/CO_2 Environments at high temperatures. J. Chem. Inf. Model. 60 (2), 700–713.
Axworthy, A.E., Dayan, V.H., Martin, G.B., 1978. Reactions of fuel-nitrogen compounds under conditions of inert pyrolysis. Fuel 57 (1), 29–35.
Bai, Z., Jiang, X.Z., Luo, K.H., 2021. Effects of water on pyridine pyrolysis: a reactive force field molecular dynamics study. Energy. 121798.
Bowman, C.T., 1992. Control of combustion-generated nitrogen oxide emissions: technology driven by regulation. Symposium (International) on Combustion. 24 (1), 859–78.
Bai, Z, Jiang, X.Z., Luo, K.H., 2023. Reactive force field molecular dynamics simulation of pyridine combustion assisted by an electric field. Fuel 333, 126455.
Döntgen, M., Przybylski-Freund, M.-D., Kröger, L.C., Kopp, W.A., Ismail, A.E., Leonhard, K., 2015. Automated discovery of reaction pathways, rate constants, and transition states using reactive molecular dynamics simulations. J. Chem. Theory Comput. 11 (6), 2517–2524.
Feng, M., Jiang, X.Z., Luo, K.H., 2019. A reactive molecular dynamics simulation study of methane oxidation assisted by platinum/graphene-based catalysts. Proc. Combust. Inst. 37 (4), 5473–5480.
Foucher, F., Higelin, P., Mounaïm-Rousselle, C., Dagaut, P., 2013. Influence of ozone on the combustion of n-heptane in a HCCI engine. Proc. Combust. Inst. 34 (2), 3005–3012.
Gao, X., Zhang, Y., Adusumilli, S., Seitzman, J.M., Sun, W., Ombrello, T., et al. (Eds.), 2015. The Effect of Ozone Addition on Flame Propagation. 53rd AIAA Aerospace Sciences Meeting.
Glarborg, P., Jensen, A., Johnsson, J.E., 2003. Fuel nitrogen conversion in solid fuel fired systems. Prog. Energy Combust. Sci. 29 (2), 89–113.
Gluckstein, M.E., Morrison, R.B., Khammash, T.B., 1955. Combustion with ozone-modification of flame speeds C_2 hydrocarbon-air mixtures.
Humphrey, W., Dalke, A., Schulten, K., 1996. VMD: visual molecular dynamics. J. Mol. Graph. 14 (1), 33–38.
Ikeda, E., Nicholls, P., Mackie, J.C., 2000. A kinetic study of the oxidation of pyridine. Proc. Combust. Inst. 28 (2), 1709–1716.
Jiang, X.Z., Luo, K.H., 2021. Reactive and electron force field molecular dynamics simulations of electric field assisted ethanol oxidation reactions. Proc. Combust. Inst. 38 (4), 6605–6613.
Jiang, X.Z., Feng, M., Zeng, W., Luo, K.H., 2019. Study of mechanisms for electric field effects on ethanol oxidation via reactive force field molecular dynamics. Proc. Combust. Inst. 37 (4), 5525–5535.
Jiang, X.Z., Luo, K.H., Ventikos, Y., 2020. Principal mode of Syndecan-4 mechanotransduction for the endothelial glycocalyx is a scissor-like dimer motion. Acta Physiol. 228 (3), e13376.
Liu, J., Guo, X., 2017. ReaxFF molecular dynamics simulation of pyrolysis and combustion of pyridine. Fuel Process. Technol. 161, 107–115.
Luo, J., Zou, C., He, Y., Jing, H., Cheng, S., 2019. The characteristics and mechanism of NO formation during pyridine oxidation in O_2/N_2 and O_2/CO_2 atmospheres. Energy 187, 115954.
Mok, Y.S., Lee, H.-J., 2006. Removal of sulfur dioxide and nitrogen oxides by using ozone injection and absorption–reduction technique. Fuel Process. Technol. 87 (7), 591–597.
Nasser, S.H., Morris, S., James, S., 1998. A novel fuel efficient and emission abatement technique for internal combustion engines. SAE Trans., 1410–1425
Nelson, P.F., Kelly, M.D., Wornat, M.J., 1991. Conversion of fuel nitrogen in coal volatiles to NOx precursors under rapid heating conditions. Fuel 70 (3), 403–407.
Senftle, T.P., Hong, S., Islam, M.M., Kylasa, S.B., Zheng, Y., Shin, Y.K., et al., 2016. The ReaxFF reactive force-field: development, applications and future directions. NPJ Comput. Mater. 2 (1), 1–14.
Solomon, P.R., Colket, M.B., 1978. Evolution of fuel nitrogen in coal devolatilization. Fuel 57 (12), 749–755.
Sun, W., Gao, X., Wu, B., Ombrello, T., 2019. The effect of ozone addition on combustion: Kinetics and dynamics. Prog. Energy Combust. Sci. 73, 1–25.
Tachibana, T., Hirata, K., Nishida, H., Osada, H., 1991. Effect of ozone on combustion of compression ignition engines. Combust. Flame 85 (3–4), 515–519.
Thompson, A.P., Aktulga, H.M., Berger, R., Bolintineanu, D.S., Brown, W.M., Crozier, P.S., et al., 2022. LAMMPS-a flexible simulation tool for particle-based materials modeling at the atomic, meso, and continuum scales. Comput. Phys. Commun. 271, 108171.
Van Duin, A.C., Dasgupta, S., Lorant, F., Goddard, W.A., 2001. ReaxFF: a reactive force field for hydrocarbons. J. Phys. Chem. A 105 (41), 9396–9409.
Weng, W., Nilsson, E., Ehn, A., Zhu, J., Zhou, Y., Wang, Z., et al., 2015. Investigation of formaldehyde enhancement by ozone addition in CH_4/air premixed flames. Combust. Flame 162 (4), 1284–1293.
Yamada, H., Yoshii, M., Tezaki, A., 2005. Chemical mechanistic analysis of additive effects in homogeneous charge compression ignition of dimethyl ether. Proc. Combust. Inst. 30 (2), 2773–2780.
Zhang, L., Duin, A.C.V., Zybin, S.V., Goddard III, W.A., 2009. Thermal decomposition of hydrazines from reactive dynamics using the ReaxFF reactive force field. J. Phys. Chem. B 113 (31), 10770–10778.
Zhang, H., Qin, H., Zhao, L., Liu, J., Wu, J., Jiang, X., 2021. One new channel for the reduction of NO during gasification condition: An insight from DFT calculations. Combust. Sci. Technol., 1–19
Zhang, Y., Zhu, M., Zhang, Z., Shang, R., Zhang, D., 2016. Ozone effect on the flammability limit and near-limit combustion of syngas/air flames with N_2, CO_2, and H_2O dilutions. Fuel 186, 414–421.
Zhang, L., Zybin, S.V., Van Duin, A.C., Dasgupta, S., Goddard III, W.A., Kober, E.M., 2009. Carbon cluster formation during thermal decomposition of octahydro-1, 3, 5, 7-tetranitro-1, 3, 5, 7-tetrazocine and 1, 3, 5-triamino-2, 4, 6-trinitrobenzene high explosives from ReaxFF reactive molecular dynamics simulations. J. Phys. Chem. A 113 (40), 10619–10640.